GIGYF2 and 4EHP Inhibit Translation Initiation of Defective Messenger RNAs to Assist Ribosome-Associated Quality Control

Kelsey L. Hickey[1], Kimberley Dickson[5], J. Zachery Cogan[1], Joseph M. Replogle[1], Michael Schoof[7], Karole N. D'Orazio[10], Niladri K. Sinha[10], Adam Frost[3,7,8], Rachel Green[2,10], Kamena K. Kostova[9,*], Jonathan S. Weissman[1,2,3,4,6,8,*]

[1]Department of Cellular and Molecular Pharmacology, University of California, San Francisco, San Francisco, CA 94158, USA

[2]Howard Hughes Medical Institute,

[3]California Institute for Quantitative Biomedical Research,

[4]Center for RNA Systems Biology,

[5]Lawerence University, Department of Biology, Appleton, WI 54911, USA

[6]Innovative Genomics Institute, University of California, Berkeley, Berkeley, CA 94720, USA

[7]Department of Biochemistry and Biophysics, University of California, San Francisco, San Francisco, CA 94158, USA

[8]Chan Zuckerberg Biohub, San Francisco, CA 94158, USA

[9]Carnegie Institution for Science, Department of Embryology, Baltimore, MD, 21218, USA

[10]Johns Hopkins University, Department of Biology, Baltimore, MD 21218, USA

[*]Corresponding authors. Email: jonathan.weissman@ucsf.edu, Kostova@carnegiescience.edu

Abstract

Ribosome-associated Quality Control (RQC) pathways protect cells from toxicity caused by incomplete protein products resulting from translation of damaged or problematic mRNAs. Extensive work in yeast has identified highly conserved mechanisms that lead to the degradation of the faulty mRNA and partially synthesized polypeptide. Here, we used CRISPR-Cas9-based screening to search for additional RQC strategies in mammals. We found that failed translation leads to specific silencing of translation initiation on that message. This negative feedback loop is mediated by two translation inhibitors, GIGYF2 and 4EHP, in part via the ribosome collision sensor ZNF598. Both model substrates and growth-based assays established that inhibition of additional rounds of translation acts in concert with known RQC pathways to prevent buildup of toxic proteins. Inability to block translation of faulty mRNAs, and subsequent accumulation of partially synthesized polypeptides, could explain the neurodevelopmental and neuropsychiatric disorders observed in mice and humans with compromised GIGYF2 function.

Translation is an enormous amplification step where each message is turned into hundreds of proteins. As a result, defective mRNAs that lead to incomplete and potentially toxic proteins jeopardize cell and organismal viability. Events such as premature polyadenylation, RNA damage or problematic sequences can cause ribosomes to stall irreversibly. To counter the threat posed by stalled ribosomes, cells have evolved multiple surveillance mechanisms that release the trapped ribosome, and degrade the faulty mRNA and the partially synthesized peptide (*1–3*). The release and subsequent proteasomal degradation of the incomplete polypeptide is mediated by the evolutionarily conserved Ribosome-associated Quality Control (RQC) pathway. Mutations of key RQC components have been associated with stress at the cellular level, and neurodegeneration at the organismal level (*4–8*), further emphasizing the importance of RQC for maintaining protein homeostasis in higher eukaryotes. Given the toxicity of partially synthesized proteins, it is possible that multiple layers of regulation exist to prevent, detect, and cope with ribosome stalling. However, our understanding of how RQC cooperates with other pathways governing protein homeostasis is incomplete.

To systematically explore how mammalian cells cope with ribosome stalling, we designed a mammalian RQC reporter that contains an open-reading frame encoding for the green fluorescent protein, but no stop codon ($GFP_{Non\text{-}stop}$). Incomplete proteins generated from such messages are model substrates for RQC-mediated degradation in yeast (*1*) but have not been studied in mammals. Upstream of the GFP, the reporter encodes BFP separated by a T2A ribosome skipping sequence (Fig. 1A), which serves as an expression control. Since messages lacking a stop codon are rapidly degraded by the exosome (*9*) we introduced a triple helix derived from the MALAT1 non-coding RNA at the 3' end to stabilize the message (*10*). When a ribosome engages the reporter, it will constitutively synthesize and release the BFP independent of stalling. Since the encoded GFP lacks a stop codon, translation through the GFP to the end of the message (Fig. S1A) causes ribosome stalling and subsequent degradation of the GFP nascent polypeptide via the RQC pathway. Wild type cells accumulate BFP, but not GFP, resulting in a substantial decrease (~ 100 fold) in the GFP/BFP ratio for the $GFP_{Non\text{-}stop}$ reporter compared to two control reporters that contain either a stop codon before the Malat1 sequence (GFP_{Stop}), or a stop codon and a canonical polyA tail (GFP_{PolyA}) (Fig. 1A, B). Knockdown of a core RQC component, *NEMF,* led to the stabilization of GFP (Fig. 1C, Fig. S1B), confirming the role of

mammalian *NEMF* in degradation of nascent polypeptides resulting from non-stop decay mRNAs (*11*).

We next used the $GFP_{Non\text{-}stop}$ reporter in a FACS-based genome-wide CRISPRi screen to gain a comprehensive view of mechanisms that cells have for minimizing accumulation of nascent polypeptides resulting from mRNAs lacking a stop codon. Specifically, we infected our reporter cell line with sgRNAs targeting each known open reading frame and used FACS followed by deep sequencing of the sgRNAs to identify genes which upon knockdown lead to accumulation of the non-stop reporter (Fig. 1D, E). As expected, the vast majority of known components from each stage of the RQC pathway (stall detection, ribosome splitting, nascent chain extraction, mRNA and peptide degradation) were among the top hits (Fig. 1E, F, S1C, D).

In addition to factors previously implicated in the RQC pathway, the screen yielded several genes with no known RQC-related function. To differentiate between factors that allow mammalian cells to cope with stalled ribosomes as part of RQC from components of parallel proteostasis pathways, we complemented our reporter-based screen with a growth-based CRISPRi screen to search for components that have synergistic growth defects in combination with loss of NEMF. This idea was motivated by recent findings that the NEMF homolog in bacteria (RqcH) has a synergistic interaction with the tmRNA/ ssrA pathway which helps dispose of incomplete translation products (*12*). We took advantage of the growth defect caused by NEMF depletion (Fig. S2A) and conducted a genome-wide screen in a compromised RQC background (Fig. 2A, S2B). We expect that depletion of RQC components will have similar effect alone or in combination with *NEMF* knockdown (buffering interaction) (Fig. S2C). On the other hand, disruption of pathways that work in parallel with RQC to degrade failed translation products are expected to exacerbate the growth phenotype caused by loss of *NEMF* (synergistic interaction).

Two genes stood out as having both a strong synergistic interaction with loss of NEMF and stabilizing effect on the RQC reporter upon knockdown (Fig. 2B); PATL1 and GIGYF2. PATL1 is a characterized scaffold protein that bridges mRNA decapping and deadenylation (*13*). Stabilization of damaged mRNAs could explain both the increased levels of stalled nascent

polypeptides and the synergistic growth interaction with *NEMF* knockdown, which disposes of incomplete protein products of such damaged mRNAs. We focused our attention on the second factor, GIGYF2, which has not been previously implicated in the cellular response to damaged messages. Overexpression studies of tagged GIGYF2 have shown that it interacts with the inhibitory cap-binding protein 4EHP (*14*) and the ubiquitin ligase ZNF598 (*15*), which is responsible for detecting ribosome collisions and targeting stalled ribosomes to RQC (*16*, *17*). We confirmed that these three factors form a complex by both mass spectrometry of ZNF598 associated factors (Fig. S3) and immunoprecipitation followed by western blot of endogenously tagged GIGYF2 (*18*) (Fig. 2C).

The screen results suggest that GIGYF2 and 4EHP function in parallel to the RQC pathway to alleviate the stalling burden in cells. To test this hypothesis, we measured the growth defect of cells expressing sgRNAs targeting *NEMF* and *GIGYF2* alone or in combination (Fig. 2D, S4A). Consistent with the genetic interaction (GI) screen results, the moderate growth phenotype imparted by knocking-down *NEMF* was exacerbated in combination with *GIGYF2* knockdown (Fig. 2D). Similarly, *4EHP* knockdown also had a synergistic interaction with *NEMF* knockdown, suggesting that GIGYF2 and 4EHP work in parallel to NEMF (Fig. 2E). In addition, *ZNF598* knockdown had buffering interactions with GIGYF2 (Fig. 2E, S4B) consistent with the data that these three proteins form a complex and work together in the same pathway.

Previous studies have shown that recruitment of GIGYF2 to a reporter mRNA results in translational repression (*15*, *19*). It has been hypothesized that GIGYF2 requires an adapter protein to be efficiently brought to its target mRNA, although the endogenous substrates and recruitment factors remain incompletely characterized. Our genetic and biochemical studies support a model where GIGYF2 and 4EHP are recruited to messages harboring stalled ribosomes by ZNF598, which ultimately leads to translational silencing of the mRNA. To test this model, we used the $GFP_{Non\text{-}stop}$ fluorescent reporter and compared the levels of BFP, which is released before stalling and is, therefore, a readout of the reporter expression levels, and GFP, which is degraded due to ribosome stalling. Unlike knockdown of RQC factors which stabilize only GFP, *GIGYF2* and *4EHP* knockdown increased both fluorescent signals (Fig. 3A). This effect was not confounded by changes in the mRNA levels (Fig. 3B), confirming that GIGYF2 and 4EHP are

translational inhibitors. To directly measure the changes in ribosome occupancy on our $GFP_{Non-stop}$ stalling reporter, we performed ribosome profiling. Consistent with the fluorescent reporter assay, the translation efficiency of the reporter was increased in both GIGYF2 and 4EHP knockdown cell lines (Fig. S5A, B). Additionally, inhibiting the proteasome further stabilized the $GFP_{Non-stop}$ in the *GIGYF2, 4EHP* and *ZNF598* knockdown cells lines, but not in *NEMF* knockdown cell lines consistent with the role of *NEMF* in UPS-mediated nascent chain degradation (Fig. 3C). This result indicates that the observed increase in fluorescence upon *GIGYF2* and *4EHP* knockdown is not caused by nascent chain stabilization, but by increased ribosome engagement, and that the partially synthesized polypeptide is still targeted for degradation by RQC.

To ensure that the observed translational effect was specific to faulty mRNAs, and not due to global changes in protein production, we used a second set of reporters with bidirectional promoters. One promoter drives GFP with a canonical stop codon and polyA tail, and the other drives a non-stop reporter ($RFP_{Non-stop}$) or a control fluorescent protein (RFP_{Stop}) on a separate mRNA. Knockdown of *NEMF*, *GIGYF2*, and *4EHP* increased the RFP/GFP ratio for $RFP_{Non-stop}$, but not RFP_{Stop} (Fig 3D). These knockdowns did not have a global effect on translation as the GFP levels were unchanged (Fig S5C). This effect was not due to changes in mRNA levels (Fig S5D), consistent with the above $GFP_{Non-stop}$ reporter. In addition, a double knockdown of *NEMF* and *GIGYF2* increased the RFP/GFP ratio to a greater extent than either single knockdown, further suggesting that these factors are components of two parallel pathways coping with ribosome stalling (Fig. 3D). We confirmed that the observed translational silencing does not depend on the type of stall by measuring the effect of *GIGYF2* and *4EHP* knockdown on previously characterized No-Go reporter, containing a stretch of 20 AAA codons as a stalling sequence (K20) (*20*). Similar to the $GFP_{Non-stop}$ reporter, knocking-down *GIGYF2* and *4EHP* led to an increase in both GFP and BFP fluorescence levels (Fig. 3E), without a change in mRNA levels (Fig. 3F).

We next explored whether GIGYF2 and/or 4EHP played a role in ribosome quality control in yeast. BLAST (*21*) search identified two homologs of GIGYF2 in yeast (Smy2p and Syh1p), and no clear candidate for a 4EHP homolog. To determine if Smy2p and Syh1p play a role in

preventing accumulation of incomplete polypeptides, we utilized a previously characterized yeast stalling reporter (*22*). This reporter expresses a no-go substrate and a control fluorescent protein from a bidirectional promoter. The stalling substrate encodes GFP separated by a T2A ribosome skipping sequence from HIS3 gene containing an internal stretch of non-optimal codons (CGA_{12}). As a control, we used a similar reporter without the CGA12 stalling sequence. We compared the protein levels by flow cytometry and found that knockout of SMY2 and SYH1 alone led to a partial increase in the GFP/RFP ratio (Fig. 3G). Deleting both homologs led to a greater increase in GFP/RFP compared to the single deletes, suggesting that Smy2p and Syh1p have redundant function. This redundancy could account for the lack of identification of these factors in the early RQC screens. In contrast to the mammalian system, the increased expression of the reporter was accompanied by mRNA stabilization (Fig. 3H). These data suggest that the role GIGYF2-like proteins play in ribosome associated quality control preceded the last common ancestor of yeast and mammals. However, the output of this response in yeast is primarily destabilization of the faulty mRNA consistent with the apparent lack of a yeast homolog of 4EHP which is an essential part of the mechanism of translation inhibition in mammals. Alternatively, Smy2p/Syh1p may mediate translational repression in yeast, which then leads to secondary mRNA decay.

Our genetic and biochemical data suggest that mammalian GIGYF2 and 4EHP can be recruited to problematic messages by the ubiquitin ligase ZNF598 (*20*, *23*) (Fig. 4A). To explore this hypothesis, we used an MS2-based system to tether ZNF598, GIGYF2, or 4EHP to a reporter mRNA (*24*). We transiently co-expressed a non-stalling reporter ($GFP_{MS2\text{-}stop}$) harboring three MS2 stem-loops in its 5' UTR together with MS2 binding protein (MS2BP) fusions in HEK293T cells. Consistent with published data, recruitment of GIGYF2 or 4EHP to the reporter led to inhibition of translation initiation (*19*), as evidenced by the robust decrease in GFP fluorescence without significant changes in the mRNA levels (Fig. 4B, Fig. S6A). Additionally, recruitment of ZNF598 to the reporter induced similar translational silencing. The translation level was not strongly affected by MS2BP recruitment alone, or overexpression of a FLAG-tagged GIGYF2 protein that does not get recruited to the reporter (Fig. S6B, C), indicating that the observed translational silencing was specific for the tethering of the factors to the mRNA.

To explore the genetic requirements for translation inhibition, we generated stable cell lines expressing an MS2-fusion protein, as well as $GFP_{MS2\text{-}stop}$ reporter, and CRISPRi machinery (Fig. 4C, S6D, E). We used CRISPRi to knock-down *ZNF598*, *GIGYF2*, or *4EHP* (Fig. S7A-C) and measured the effect of the knockdown on translational inhibition via flow cytometry. We found that the decrease in GFP fluorescence caused by MS2-ZNF598 recruitment was alleviated in cells lacking GIGYF2 or 4EHP (Fig. 4D, S7D). Lower expression of the MS2BP-GIGYF2 fusion protein in K562 cells resulted in an attenuated repression phenotype compared to HEK293T (Fig. S6E). Nonetheless, the GIGYF2-mediated repression depended on 4EHP. Similarly, 4EHP-mediated repression depended on GIGYF2, suggesting that these two factors act together to mediate translation inhibition (Fig. 4D, S7E, F). By contrast, neither silencing by GIGYF2, nor by 4EHP were impacted by knockdown of ZNF598 when these factors were directly recruited to the mRNA, indicating that GIGYF2 and 4EHP work downstream of ZNF598. These epistasis experiments support a model where ZNF598 serves as a scaffold that could recruit GIGYF2 and 4EHP to faulty mRNAs.

ZNF598 recognizes collided stalled ribosomes and ubiquitinates the small subunit of the ribosome, which triggers ribosome splitting and subsequent RQC complex engagement (*16*, *25*). We next tested whether ZNF598-mediated ubiquitination is required for recruitment of GIGYF2 and 4EHP to the mRNA. We generated ubiquitination-deficient MS2BP-ZNF598 fusion proteins that harbored inactivating mutations in the RING domain (C29A) or deletions of the entire domain (ΔRING) and compared their ability to translationally silence the $GFP_{MS2\text{-}stop}$ reporter (*23*). Surprisingly, both mutants were capable of repressing translation (Fig. 4E, S8A). Recruitment of a stably integrated MS2BP-ZNF598ΔRING also repressed translation in a GIGYF2 and 4EHP-dependent manner matching the wildtype ZNF598 recruitment. (Fig. 4F, S8B). These data suggest that ZNF598 has a dual function when it engages collided ribosomes. It serves as a ubiquitin ligase that mono-ubiquitinates the 40S small subunit, triggering release of the stalled ribosome and subsequent RQC engagement, and nascent polypeptide degradation (*16*, *23*). In addition, ZNF598 also serves as a scaffold that recruits GIGYF2 and 4EHP to the mRNA, in a ubiquitination independent manner. Once recruited, GIGYF2 and 4EHP sequester the mRNA cap, blocking ribosome initiation, and decreasing the translational load on problematic messages (Fig. 4G). However, the translation inhibition phenotype of ZNF598 knockdown is

consistently weaker than GIGYF2 knockdown (Fig. 3A). Additionally, the double GIGYF2 and ZNF598 knockdown inhibits translation to a similar level as GIGYF2 alone. Taken together, these data suggest that there are both ZNF598-dependent and ZNF598-independent mechanisms for recruitment of GIGYF2 and 4EHP to mediate translation inhibition on defective messages (Fig. 4G).

The cell faces an inherent challenge in detecting problematic mRNAs in that it is only through the act of translation itself that the lesion can be recognized. Our work reveals a novel mechanism in which failed translation leads to inhibition of further translation initiation on that message. This pathway acts in parallel with previously described quality control pathways, which trigger mRNA degradation, ribosome release, and proteasomal degradation of the stalled nascent polypeptide. Without a mechanism to block further initiation on problematic messages, translation of faulty mRNAs would continue for as long as the message persists. GIGYF2 and 4EHP enable the cell to break this cycle by allowing a failed translation event to initiate a specific negative feedback loop which shuts down further translation of the message. Although GIGYF2 and 4EHP have been implicated in translational control in a number of different settings (*14*, *15*, *19*, *26*, *27*), our data argue that faulty mRNAs that cause ribosome stalling comprise an important subset of endogenous substrates for GIGYF2 and 4EHP mediated repression. Indeed, we see loss of GIGYF2 stabilizes two distinct classes of stalling reporters. Moreover, knocking down *GIGYF2* in combination with RQC components had a strong synergistic growth interaction in the absence of a reporter, suggesting that there is a continuous production of endogenous stalling substrates. Loss of GIGYF2 has been associated with neurodegenerative and neurodevelopmental phenotypes (*28*, *29*), similar to loss of RQC components (*30*). It is tempting to speculate that dysregulation of the GIGYF2/4EHP pathway increases the burden on the proteostasis network in neurons leading to cell stress and/or death.

1. M. H. Bengtson, C. A. P. Joazeiro, Role of a ribosome-associated E3 ubiquitin ligase in protein quality control. *Nature*. **467**, 470–473 (2010).
2. T. Inada, H. Aiba, Translation of aberrant mRNAs lacking a termination codon or with a shortened 3?-UTR is repressed after initiation in yeast. *EMBO J.* **24**, 1584–1595 (2005).
3. S. Ito-Harashima, K. Kuroha, T. Tatematsu, T. Inada, Translation of the poly(A) tail plays crucial roles in nonstop mRNA surveillance via translation repression and protein destabilization by proteasome in yeast. *Genes Dev.* **21**, 519–24 (2007).
4. O. Brandman, J. Stewart-Ornstein, D. Wong, A. Larson, C. C. Williams, G.-W. Li, S. Zhou, D. King, P. S. Shen, J. Weibezahn, J. G. Dunn, S. Rouskin, T. Inada, A. Frost, J. S. Weissman, A ribosome-bound quality control complex triggers degradation of nascent peptides and signals translation stress. *Cell*. **151**, 1042–54 (2012).
5. R. Verma, R. S. Oania, N. J. Kolawa, R. J. Deshaies, Cdc48/p97 promotes degradation of aberrant nascent polypeptides bound to the ribosome. *Elife*. **2**, e00308 (2013).
6. Q. Defenouillère, Y. Yao, J. Mouaikel, A. Namane, A. Galopier, L. Decourty, A. Doyen, C. Malabat, C. Saveanu, A. Jacquier, M. Fromont-Racine, Cdc48-associated complex bound to 60S particles is required for the clearance of aberrant translation products. *Proc. Natl. Acad. Sci. U. S. A.* **110**, 5046–51 (2013).
7. S. Shao, K. Von der Malsburg, R. S. Hegde, Listerin-dependent nascent protein ubiquitination relies on ribosome subunit dissociation. *Mol. Cell*. **50**, 637–648 (2013).
8. S. Shao, R. S. Hegde, Reconstitution of a Minimal Ribosome-Associated Ubiquitination Pathway with Purified Factors. *Mol. Cell*. **55**, 880–90 (2014).
9. P. A. Frischmeyer, A. Van Hoof, K. O'Donnell, A. L. Guerrerio, R. Parker, H. C. Dietz, An mRNA surveillance mechanism that eliminates transcripts lacking termination codons. *Science (80-.).* (2002), doi:10.1126/science.1067338.
10. J. E. Wilusz, C. K. JnBaptiste, L. Y. Lu, C.-D. Kuhn, L. Joshua-Tor, P. A. Sharp, A triple helix stabilizes the 3' ends of long noncoding RNAs that lack poly(A) tails. *Genes Dev.* **26**, 2392–407 (2012).
11. S. Shao, A. Brown, B. Santhanam, R. S. Hegde, Structure and Assembly Pathway of the Ribosome Quality Control Complex. *Mol. Cell*. **57**, 433–444 (2015).
12. I. Lytvynenko, H. Paternoga, A. Thrun, A. Balke, T. A. Müller, C. H. Chiang, K. Nagler, G. Tsaprailis, S. Anders, I. Bischofs, J. A. Maupin-Furlow, C. M. T. Spahn, C. A. P. Joazeiro, Alanine Tails Signal Proteolysis in Bacterial Ribosome-Associated Quality Control. *Cell*. **178**, 76-90.e22 (2019).
13. S. Ozgur, M. Chekulaeva, G. Stoecklin, Human Pat1b Connects Deadenylation with mRNA Decapping and Controls the Assembly of Processing Bodies. *Mol. Cell. Biol.* **30**, 4308–4323 (2010).
14. D. Peter, R. Weber, F. Sandmeir, L. Wohlbold, S. Helms, P. Bawankar, E. Valkov, C. Igreja, E. Izaurralde, GIGYF1/2 proteins use auxiliary sequences to selectively bind to 4EHP and repress target mRNA expression. *Genes Dev.* **31** (2017), doi:10.1101/gad.299420.117.
15. M. Morita, L. W. Ler, M. R. Fabian, N. Siddiqui, M. Mullin, V. C. Henderson, T. Alain, B. D. Fonseca, G. Karashchuk, C. F. Bennett, T. Kabuta, S. Higashi, O. Larsson, I. Topisirovic, R. J. Smith, A.-C. Gingras, N. Sonenberg, A Novel 4EHP-GIGYF2 Translational Repressor Complex Is Essential for Mammalian Development. *Mol. Cell. Biol.* **32**, 3585–3593 (2012).

16. S. Juszkiewicz, V. Chandrasekaran, Z. Lin, S. Kraatz, V. Ramakrishnan, R. S. Hegde, ZNF598 Is a Quality Control Sensor of Collided Ribosomes Correspondence. *Mol. Cell*. **72**, 469–481 (2018).
17. Y. Matsuo, K. Ikeuchi, Y. Saeki, S. Iwasaki, C. Schmidt, T. Udagawa, F. Sato, H. Tsuchiya, T. Becker, K. Tanaka, N. T. Ingolia, R. Beckmann, T. Inada, Ubiquitination of stalled ribosome triggers ribosome-associated quality control. *Nat. Commun.* **8**, 159 (2017).
18. M. D. Leonetti, S. Sekine, D. Kamiyama, J. S. Weissman, B. Huang, H. P. Babcock, P. De Camilli, A scalable strategy for high-throughput GFP tagging of endogenous human proteins, doi:10.1073/pnas.1606731113.
19. M.-H. Kryszke, B. Adjeriou, F. Liang, H. Chen, F. Dautry, "Post-transcriptional gene silencing activity of human GIGYF2" (2016), , doi:10.1016/j.bbrc.2016.05.022.
20. S. Juszkiewicz, R. S. Hegde, Initiation of Quality Control during Poly(A) Translation Requires Site-Specific Ribosome Ubiquitination. *Mol. Cell*. **65**, 743-750.e4 (2017).
21. S. F. Altschul, W. Gish, W. Miller, E. W. Myers, D. J. Lipman, Basic local alignment search tool. *J. Mol. Biol.* **215**, 403–410 (1990).
22. K. N. D'Orazio, C. C.-C. Wu, N. Sinha, R. Loll-Krippleber, G. W. Brown, R. Green, The endonuclease Cue2 cleaves mRNAs at stalled ribosomes during No Go Decay. *Elife*. **8** (2019), doi:10.7554/eLife.49117.
23. E. Sundaramoorthy, M. Leonard, R. Mak, J. Liao, A. Fulzele, E. J. Bennett, ZNF598 and RACK1 Regulate Mammalian Ribosome-Associated Quality Control Function by Mediating Regulatory 40S Ribosomal Ubiquitylation. *Mol. Cell*. **65**, 751-760.e4 (2017).
24. E. Bertrand, P. Chartrand, M. Schaefer, S. M. Shenoy, R. H. Singer, R. M. Long, Localization of ASH1 mRNA Particles in Living Yeast. *Mol. Cell*. **2**, 437–445 (1998).
25. K. Ikeuchi, P. Tesina, Y. Matsuo, T. Sugiyama, J. Cheng, Y. Saeki, K. Tanaka, T. Becker, R. Beckmann, T. Inada, Collided ribosomes form a unique structural interface to induce Hel2-driven quality control pathways. *EMBO J.* **38** (2019), doi:10.15252/embj.2018100276.
26. C. C. Amaya Ramirez, P. Hubbe, N. Mandel, J. Béthune, 4EHP-independent repression of endogenous mRNAs by the RNA-binding protein GIGYF2. *Nucleic Acids Res.* (2018), doi:10.1093/nar/gky198.
27. R. Fu, M. T. Olsen, K. Webb, E. J. Bennett, J. Lykke-Andersen, Recruitment of the 4EHP-GYF2 cap-binding complex to tetraproline motifs of tristetraprolin promotes repression and degradation of mRNAs with AU-rich elements. *RNA*. **22**, 373–382 (2016).
28. N. Krumm, T. N. Turner, C. Baker, L. Vives, K. Mohajeri, K. Witherspoon, A. Raja, B. P. Coe, H. A. Stessman, Z.-X. He, S. M. Leal, R. Bernier, E. E. Eichler, Excess of rare, inherited truncating mutations in autism. *Nat. Genet.* **47**, 582–8 (2015).
29. S. B. Thyme, L. M. Pieper, E. H. Li, S. Pandey, Y. Wang, N. S. Morris, C. Sha, J. W. Choi, K. J. Herrera, E. R. Soucy, S. Zimmerman, O. Randlett, J. Greenwood, S. A. McCarroll, A. F. Schier, Phenotypic Landscape of Schizophrenia-Associated Genes Defines Candidates and Their Shared Functions. *Cell*. **177**, 478-491.e20 (2019).
30. J. Chu, N. A. Hong, C. A. Masuda, B. V. Jenkins, K. A. Nelms, C. C. Goodnow, R. J. Glynne, H. Wu, E. Masliah, C. A. P. Joazeiro, S. A. Kay, A mouse forward genetics screen identifies LISTERIN as an E3 ubiquitin ligase involved in neurodegeneration. *Proc. Natl. Acad. Sci.* **106**, 2097–2103 (2009).

Figure Legends

Fig. 1. Genome-wide CRISPRi screen for mammalian RQC components. (**A)** Diagrams of non-stop stalling reporter ($GFP_{Non\text{-}stop}$) and control reporters (GFP_{Stop} and GFP_{PolyA}) **(B**) Relative GFP/BFP ratio of cells transiently expressing stalling or control reporters (median ± SD, N=3). (**C)** $GFP_{Non\text{-}stop}$ fluorescence level in control or *NEMF* knockdown cells. **(D**) Workflow of FACS-based CRISPRi screen. (**E**) Volcano plot of GFP stabilization phenotype and Mann-Whitney P-values from genome-scale CRISPRi FACS screen. Negative controls are shown in lavender, targeting guides in grey, and previously characterized RQC factors are labeled with unique colors. (**F**) Model of the mammalian RQC pathway with screen hits highlighted.

Fig. 2. GIGYF2 and 4EHP are components of a pathway parallel to the RQC pathway. (**A**) Genetic interaction (GI) screen for factors affecting the growth of control or *NEMF* knockdown cells. GI scores were derived by fitting the data to a quadratic curve (red dashed line) and calculating the distance of each point from the best-fit line. Genes exhibiting synergistic interactions with *NEMF* knockdown vs. control knockdown (negative GI score) are marked in blue, and genes with positive GI score (buffering interactions) are in yellow. (**B**) Cross comparison of FACS and GI CRISPRi screens. Hits from FACS screen (log2 enrichment > 1) that stabilized $GFP_{Non\text{-}stop}$ reporter upon individual re-testing are labeled and colored by GI score. (**C**) Coimmunoprecipitation (CO-IP) and immunoblot (IB) for endogenously tagged GIGYF2, and its binding partners, ZNF598 and 4EHP. (**D**) Competition assay between control cells and cells harboring a single or double knockdown of *NEMF* and *GIGYF2* (mean ± SD, N=2). The expected ratio of infected and uninfected cells is plotted in a dashed grey line. The observed synergistic interaction is shaded in grey. (**E**) Competition assay of double knockdown cell lines. The difference in the measured (actual) growth defect and additive value of single growth defects (expected) on day 16 are plotted.

Fig. 3. GIGYF2 and 4EHP selectively inhibit translation of messages harboring stalled ribosomes. (A, B, E, F) Protein, and mRNA levels for $GFP_{Non\text{-}stop}$ or K20 stalling reporters in knockdown cell lines measured by flow cytometry (median ± SD, N=2) and qPCR (mean ± SD, N=3). (**C**) BFP and GFP protein stabilization upon proteasome inhibition (t_{3h}/t_{0h}) measured by

flow cytometry (median ± SD, N=3). (**D)** Cumulative distribution plot of RFP/GFP protein ratios for reporters expressed from a bidirectional promoter in knockdown cells lines. (**G**) Box plot of GFP/RFP normalized no-go decay (NGD) or control reporter levels in knockout yeast strains measured by flow cytometry. (**H**) mRNA levels for control or no-go decay reporter in wild type or knockout strains measured by qPCR (mean ± SD, N=3).

Fig. 4. Translational inhibition by ZNF598 is mediated by GIGYF2 and 4EHP in ubiquitination-independent manner. (**A**) Model for GIGYF2 and 4EHP recruitment to mRNA by ZNF598. (**B**) Relative fluorescence of $GFP_{MS2\text{-}stop}$ reporter transiently expressed in HEK293T cells alone or with MS2BP-fusion proteins (mean ± SD, N=3) (**C**) GFP fluorescence of K562 cells stably expressing $GFP_{MS2\text{-}stop}$ reporter alone or in combination with MS2BP-fusion proteins. (**D, F**) MS2-fusion protein is recruited to the $GFP_{MS2\text{-}stop}$ reporter in control cells or knockdown cells for ZNF598, GIGYF2 or 4EHP. The effect of the knockdown on the ability of the fusion protein to silence translation from the reporter is measured via the change in GFP fluorescence. (**E**) GFP fluorescence of $GFP_{MS2\text{-}stop}$ reporter upon recruitment of wild type (wt) or ubiquitination deficient (C29A and ΔRING) ZNF598 (mean ± SD, N=3). (F) (**G**) Model of translation inhibition upon ribosome stalling in mammalian cells.

Materials and Methods:

Cell culture

K562 cells were grown in RPMI-1640 with 25mM HEPES, 2.0 g/L NaHCO3, 0.3 g/L L-Glutamine supplemented with 10% FBS, 2 mM glutamine, 100 units/mL penicillin and 100 µg/mL streptomycin. HEK293T cells were grown in Dulbecco's modified eagle medium (DMEM) in 10% FBS, 2 mM glutamine, 100 units/mL penicillin and 100 µg/mL streptomycin.

Generation of cell lines:

To generate the K562 cell line stably expressing dCas9-KRAB, WT K562 cells were stably transduced with a lentiviral vector expressing dCas9-BFP-KRAB from an EF1-a promoter with an upstream ubiquitous chromatin opening element (SFFV-dCas9-BFP-KRAB, Addgene #85969) and selected for BFP-positive cells using two rounds of fluorescence activated cell sorting (FACS) on a BD FACSAria2.

Reporter cell lines ($GFP_{Non\text{-}stop}$, GFP_{Stop}, GFP_{PolyA}, K20, $RFP_{Non\text{-}stop}$, RFP_{Stop}, $GFP_{MS2\text{-}stop}$, MS2BP, MS2BP-ZNF598, MS2BP-GIGYF2, MS2BP-4EHP) were stably transduced using Piggy-Bac transposition (System Biosciences PB210PA-1 and corresponding Piggy-Bac expression vector Table 1). Positive cells were isolated by FACS on a BD FACSAria2.

Transient expression of reporters ($GFP_{Non\text{-}stop}$, GFP_{Stop}, GFP_{PolyA}, MS2BP, MS2BP-ZNF598, MS2BP-GIGYF2, MS2BP-4EHP) was achieved by transfecting HEK293T cells with vectors from Table 1 using TransIT-LTI Transfection Reagent (Mirus, MIR 2306) according to the manufacturer's instructions.

Individual gene knockdowns were carried out by selecting sgRNA protospacers from compact hCRISPRi-v2 library and cloning them into lentiviral plasmid pU6-sgRNA EF1α-puro-t2a-BFP (Addgene 60955) as previously described (Horlbeck et al., 2016). Protospacer sequences used for individual knockdowns are listed in Table 2. The resulting sgRNA expression vectors were packaged into lentivirus by transfecting HEK293T with standard packaging vectors using TransIT-LTI Transfection Reagent (Mirus, MIR 2306). The viral supernatant was harvested 2–3

days after transfection and filtered through 0.45 μm PVDF filter and/or frozen prior to transduction into CRISPRi knockdown cell lines described above.

GFP11-GIGYF2 tagged HEK293T cells were generated as previously described (Leonetti *et al*., PNAS, 2016), using targeting sgRNA (AATACGGAACAGAATGGCAG) and ssDNA oligo(TATTTTTCTCGTTAACAGGTTTCTTCACATATAAAAATCTATTGTAAAAATACG GAAAAGAatgcgtgaccacatggtccttcatgagtatgtaaatgctgctgggattacaGGCGGTGGAGGGAGTggcgg aggtGGATCCGCAGCGGAAACGCAGACACTGAACTTTGGGCCTGAATGGTGAGTTTTC AAAATCTCAT).

Genome-scale CRISPRi screening:

Genome-scale screens were conducted similar to previously described screens (Gilbert et al., 2014; Horlbeck et al., 2016). The CRISPRi compact library (5 sgRNA/TSS) CRISPRi-v2 (Addgene, Cat#83969) were transduced in duplicate into K562 CRISPRi cells at MOI < 1 (percentage of transduced cells 2 days after transduction: 20%–40%). Replicates were maintained separately in 1.5 L of RPMI-1640 in 3 L spinner flasks for the course of the screen. 2 days after transduction, the cells were selected with 1 mg/mL puromycin for 2 days, at which point transduced cells accounted for 80%–95% of the population. Cells were allowed to recover to > 80% cell viability, as measured on an Accuri bench-top flow cytometer (BD BioSciences). The cells were maintained in spinner flasks by daily dilution to $0.5 \cdot 10^6$ cells /mL at an average coverage of greater than 1000 cells per sgRNA for the duration of the screen.

FACS based screen

Cells were sorted using BD FACS Aria2 2 days after recovery based on GFP fluorescence of $GFP_{Non\text{-}stop}$ reporter. Cells with the highest (~30%) and lowest (~30%) GFP expression were collected and frozen after collection. Approximately 30 million cells were collected per group. Genomic DNA was isolated from frozen cells, and the sgRNA-encoded regions were enriched, amplified, and prepared for sequencing as described previously (Gilbert et al., 2014).

Growth based Screen

Prior to CRISPRi-v2 library infection, K562 CRISPRi cells were infected with control sgRNA or sgRNA targeting NEMF that expressed RFP as a marker. RFP positive cells were sorted on a BD FACSAria2.

Sequencing reads were aligned to the CRISPRi v2 library sequences, counted, and quantified using the Python-based ScreenProcessing pipeline (https://github.com/mhorlbeck/ScreenProcessing; Horlbeck et al., 2016). Generation of negative control genes and calculation of phenotypes and Mann-Whitney p-values was performed as described previously (Gilbert et al., 2014; Horlbeck et al., 2016). GFP phenotypes were calculated from the top 30% sorted samples, divided by the bottom 30%. Phenotypes from sgRNAs targeting the same gene were collapsed into a single GFP stabilization phenotype using the average of the top three scoring sgRNAs (by absolute value) and assigned a p-value using the Mann-Whitney test of all sgRNAs targeting the same gene compared to the non-targeting controls. All additional CRISPR screen data analyses were performed in Python 2.7 using a combination of Numpy (v1.12.1), Pandas (v0.17.1), and Scipy (v0.17.0). For all experiments, details of quantification and statistical methods used are described in the corresponding figure legends or results sections. Gene-level phenotypes are available in Tables S4-S5.

Individual evaluation of sgRNA phenotypes:

For individual evaluation and re-testing of sgRNA phenotypes, sgRNA protospacers targeting NEMF, GIGYF2, EIF4E2, or ZNF598 or a non-targeting control protospacer (neg_ctrl-1) were individually cloned by annealing complementary synthetic oligonucleotide pairs (Integrated DNA Technologies) with flanking BstXI and BlpI restriction sites and ligating the resulting double-stranded segment into either BstXI/BlpI-digested pCRISPRia-v2 (marked with a puromycin resistance cassette and RFP similar to Horlbeck et al., 2016) or BstXI/BlpI-digested pU6-sgRNA EF1a-puro-t2a-mCherry (marked with a puromycin resistance cassette and RFP). Protospacer sequences used for individual evaluation are listed in Table 2. The resulting sgRNA expression vectors were individually packaged into lentivirus. These sgRNA vectors were transduced into K562-dCas9 cells expressing $GFP_{Non\text{-}stop}$ at MOI < 1 (20 – 40% infected cells). BFP and GFP protein levels were measured by flow cytometry at day 5 post infection. Median

fluorescent values were calculated for each cell line using FlowJo software and compared to uninfected levels.

Internally controlled growth assays:

sgRNA and double sgRNA growth phenotypes were performed by transducing cells with sgRNA expression constructs (mU6-sgRNA1 hU6-sgRNA2-puro-t2a-mCherry) at MOI < 1 (15 – 30% infected cells). The fraction of sgRNA-expressing cells was measured from 4-16 days after infection by flow cytometry on an LSR-II (BD Biosciences). A population of infected cells was selected to purity with puromycin (1 mg/mL), allowed to recover for 1 day, and harvested for measurement of mRNA levels by RT-qPCR (see below). Experiments were performed in duplicate from the infection step. The expected double phenotype score was calculated by adding the phenotype of both genes on day 16.

Epistasis was measured by subtracting the expected phenotype from the measured phenotype of those combined knockdowns.

Ribosome Profiling:

K562-dCas9 cell line stably expressing $GFP_{Non\text{-}stop}$ was infected with lenti vectors containing a guide RNA against one gene or non-targeting guide RNA (Table 2). Cells were selected using FACS to recover cells containing sgRNA (labeled with RFP). Cyclohexamide was added (100mg/ul) to the cells and they were incubated for 5 minutes at 37 °C and then pelleted at 400g for 5 minutes. Media was removed and cell pellets were immediately snap frozen. Libraries were prepared according to McGlincy and Ingolia, Methods, 2017.

RNA sequencing:

RNA was extracted using Zymo mini RNA prep (R2053) and libraries were cloned using Illumnia true stranded total RNA seq kit (20020596).

Ribosome profiling and RNAseq analysis:

Ribosome profiling and RNA-seq libraries were sequenced on an Illumina HiSeq 4000 as single end 50-bp reads (UCSF Center for Advanced Technology) at a depth of 22-64 million reads per library. Ribosome profiling reads were processed by removing 3' linker sequences using *FASTX*

clipper and de-multiplexed using *FASTX barcode splitter* (http://hannonlab.cshl.edu/fastx_toolkit/). Sample barcodes and unique molecular identifiers were trimmed using a custom Python script. Next, abundant reads were filtered by aligning to a custom library of human rRNAs, tRNAs, and primer sequences using *bowtie* v1.2 (http://bowtie-bio.sourceforge.net/). All remaining reads were aligned to a modified human genome (GRCh38.92 with addition of our CRISPRi construct and the $GFP_{Non\text{-}stop}$) using *tophat* v2.1.1 (https://ccb.jhu.edu/software/tophat/; relevant parameters: --read-mismatches=1 and --no-novel-juncs). After alignment, uniquely mapping reads were extracted, and *plastid* (https://plastid.readthedocs.io) was used to obtain gene-level read counts and normalized counts, reads per kilobase per million mapped reads (RPKM). To assign reads to genomic positions, a p-site offset of 12 nucleotides was determined by calculating the average distance of the start codon peak from the start codon (*plastid psite*). To assess the quality of the ribosome profiling data, we confirmed that the aligned reads displayed the expected three nucleotide periodicity (phasing) and that the majority of ribosome footprints had a length of 28-31 bp for all libraries. We also confirmed that the CRISPRi system produced robust target knockdown on the day of the experiment at the level of ribosome footprints (knockdown of target genes >88% for all genes). The RNA-seq libraries were processed using the same pipeline as the ribosome profiling libraries, with the exception that *tophat* was run with –read-mismatches=2 due to the longer RNAseq read length. All downstream analyses were performed using the Python libraries pandas, plastid, matplotlib, seaborn, numpy, and scipy.

For Figure S1A, footprints from K562 CRISPRi cells bearing non-targeting sgRNA are plotted as reads per million. Here, we plotted all aligned reads rather than uniquely aligned reads to visualize read density in the $GFP_{Non\text{-}stop}$ MALAT1 triple helix, which is identical to the endogenous MALAT1 lncRNA. To confirm that the reads aligning to the MALAT1 triple helix in the $GFP_{Non\text{-}stop}$ are not derived from the endogenous MALAT1 lncRNA, we performed ribosome profiling in a K562 CRISPRi cell line without the $GFP_{Non\text{-}stop}$ reporter. Here, we found that the endogenous MALAT1 background rate was <10% of the $GFP_{Non\text{-}stop}$ footprints in the MALAT1 triple helix, suggesting that the $GFP_{Non\text{-}stop}$ triple helix is indeed translated. For Figure S5A, translational efficiencies were calculated by normalizing the $GFP_{Non\text{-}stop}$ GFP ribosome footprint rpm to the $GFP_{Non\text{-}stop}$ RNAseq rpm.

RT-qPCR:

Total RNA was isolated from frozen cell samples using TRIzol reagent (Thermo Fisher Scientific) and Phase Lock Gel tubes (VWR), treated with Turbo DNase (Thermo Fisher Scientific), or using Direct-zol RNA MiniPrep kit. Reverse-transcription was carried using M-MLV (Thermo Fisher Scientific) or SSIII Reverse-transcriptase (Thermo Fisher Scientific) with random hexamer primers (Thermo Fisher Scientific, SO124) in the presence of RNaseIN Recombinant Ribonuclease Inhibitor (Thermo Fisher Scientific). Quantitative PCR (qPCR) was performed with Kappa Sybr Fast qPCR 2x Mix (Roche), according to the manufacturer's instructions on a LightCycler 480 Instrument (Roche). Experiments were performed in technical triplicates. RT-qPCR primers used are listed in (Table 3).

Immunoprecipitation and western blot:

Cells were lysed in buffer containing 10mM Tris 7.5, 150 mM NaCl, 0.5% NP-40, 5 mM Mg_2Cl, and 1x Halt™ Protease Inhibitor Cocktail (Thermo Fisher Scientific). The lysates were cleared by centrifugation at 20,000 x g for 10 min and bound to GFP-Trap Magnetic Beads (Chrometech) for 2h at 4 °C. Beads were washed 3 times with IP Buffer (10mM Tris 7.5, 150 mM NaCl, 0.1% NP-40, 5 mM Mg_2Cl). Bound material was eluted by boiling in Laemmli Buffer for 10 min at 90°C.

Proteins were separated on Bolt® 4-12% Bis-tris gels (Thermo Fisher Scientific), transferred to PVDF membrane using the Mini Trans-Blot Cell (Bio-Rad) according to the manufacturer's instructions, blocked with 5% milk in TBS, and subsequently probed. Rabbit anti ZNF598 antibody (Bethyl Laboratories, A305-108A-T), rabbit anti GIGYF2 antibody (Bethyl Laboratories, A303-731A-M), and rabbit anti 4EHP antibody (Cell Signaling, 6916S) primary antibodies were used. LI-COR IRDye800/IRDye700 anti-rabbit (Odyssey) secondary antibody was used at 1:10,000 dilution. All blots were visualized using the LI-COR (Odyssey) system.

ZNF598 Mass Spectrometry:

Cell lines

3X-FLAG-tagged ZNF598 overexpressing (ZNF598-OE) Flp-In T-Rex 293 cells (kind gift from Dr. Nahum Sonenberg and Dr. Thomas Tuschl, Garzia *et al.*, Nature Communications, 2017)

were grown in high-glucose Dulbecco's Modified Eagle Medium (Thermo Fisher, 11995040, containing 4 mM L-Glutamine and 1 mM sodium pyruvate) supplemented with 10% (v/v) fetal bovine serum. The affinity purification mass spectrometry experiment was performed in biological triplicate. Two million low-passage cells were seeded per 10 cm dish. Expression of 3X-FLAG-tagged ZNF598 was induced (24 hours post seeding) for 24 hours by the addition of doxycycline at 1 µg/ml at final concentration.

FLAG-immunoprecipitation of 3X-FLAG-ZNF598 from HEK293 cells

Cells were washed with warm PBS (containing 360 µM emetine), and harvested in ice-cold lysis buffer (50 mM TRIS pH 8.0, 150 mM KCl, 15 mM $MgCl_2.6H_2O$, 5% glycerol) supplemented with 1% Triton X-100, 360 µM emetine, 20 mM N-ethylmaleimide, 80 units TURBO DNase (Thermo Fisher, AM2238) and protease inhibitors (cOmplete Protease Inhibitor Cocktail, Roche; Protease Inhibitor Cocktail, Millipore Sigma; and PMSF, Millipore Sigma). Cell lysates were clarified in a tabletop micro-centrifuge (15 minutes, 4°C). Equal protein amounts from the clarified supernatant were used for each immunoprecipitation. The clarified supernatant was incubated with ANTI-FLAG-Agarose M2 affinity gel (Millipore Sigma #A2220, 15 µl of packed affinity resin) for 1 hour, washed four times with 400 µl wash 1 buffer (lysis buffer supplemented with 0.1% Triton X-100 and 360 µM emetine), then washed four times with wash 2 buffer (50 mM TRIS pH 8.0, 150 mM KCl, 15 mM $MgCl_2.6H_2O$ supplemented with 360 µM emetine), and eluted in 80 µl elution buffer (50 mM TRIS pH 8.0, 150 mM KCl, 15 mM $MgCl_2.6H_2O$ supplemented with 400 µg/ml 3X FLAG-peptide (Millipore Sigma, #F4799)). Eluates were flash frozen in liquid nitrogen and stored at -80°C prior to protein digestion.

Protein Digestion

Protein extracts (4 µg) were diluted up to 300 µl in 10 mM triethyl ammonium bicarbonate (TEAB) and were reduced with 15 µl of 7.5 mg/ml DL-dithiothreitol (DTT) (60°C, 1 hour). After cooling to room temperature, samples were alkylated with 15 µl of 18.5 mg/ml iodoacetamide for 15 minutes at room temperature in the dark. Reduced and alkylated proteins were buffer-exchanged on a 30 kDa molecular weight spin cartridge (Amicon Ultra 0.5 ml, Millipore Sigma) and washed four times with 400 µl 10 mM TEAB. Proteins were digested overnight at 37°C on the filter with 300 µl Trypsin (20 µg in 3 ml 10 mM TEAB, Promega

Sequencing Grade Modified Trypsin). Additional Trypsin (100 µl of 10 mg/ml) was added the next morning (37°C, 1 hour). Peptides were removed from the top of the filter and the filter was washed twice with 300 2% acetonitrile, 0.1% formic acid. All washes were combined and dried.

Liquid Chromatography and Mass Spectrometry

Liquid Chromatography and Mass Spectrometry was performed at the Mass Spectrometry and Proteomics Core, JHMI. Peptides were analyzed by liquid chromatography interfaced with tandem mass spectrometry (LC/MS/MS) using a Waters nanoACQUITY UPLC system (www.waters.com) interfaced with an Orbitrap Fusion™ Lumos™ Tribrid™ Mass Spectrometer (www.thermofisher.com). Fractions were resuspended in 20 µl loading buffer (2% acetonitrile in 0.1% formic acid) and analyzed by reverse phase liquid chromatography coupled to tandem mass spectrometry. Peptides (50%, approx. 1 µg) were loaded onto a C18 trap (S-10 µM, 120 Å, 75 µm x 2 cm, YMC, Japan) and subsequently separated on an in-house packed PicoFrit column (75 µm x 200 mm, 15u, +/-1 µm tip, New Objective) with C18 phase (ReproSil-Pur C18-AQ, 3 µm, 120 Å, www.dr-maisch.com) using 2-90% acetonitrile gradient at 300 nl/min over 120 min. Eluting peptides were sprayed at 2.0 kV directly into the Lumos.

Survey scans (full MS) were acquired from 350-1800 m/z with data-dependent monitoring with a 3 sec cycle time. Each precursor individually isolated in a 1.6 Da window and fragmented using HCD activation collision energy 30 and 15 sec dynamic exclusion, first mass being 120 m/z. Precursor and fragment ions were analyzed at resolutions 120,000 and 30,000, respectively, with automatic gain control (AGC) target values at 4e5 with 50 ms maximum injection time (IT) and 1e5 with 100 ms maximum IT, respectively.

Processing of Mass Spectrometry Data

Raw data was processed and analyzed using the MaxQuant software suite (Cox and Mann, Nature Biotechnology, 2008). Default settings were used except that 'Match between runs' was turned on to transfer peptide identification from an LC-MS run, in which the peptide has been identified by MS/MS, to another LC-MS run, in which no MS/MS data for the same peptide was acquired or no peptide was assigned (Tyanova *et al.*, Nature Methods, 2016). Search parameters were as follows:

a maximum of two missed cleavages were allowed, cysteine carbamidomethyl was included as a fixed modification, and variable modifications included oxidation of methionine, protein N-terminal acetylation, deamidation of glutamine and asparagine, phosphorylation of serine, threonine and tyrosine, and Gly-Gly ubiquitin remnant on lysine. Database search was performed with Andromeda (Cox and Mann, Nature Biotechnology, 2008; Cox et al., Journal of Proteomic Research, 2011) against Uniprot human database (UP000005640_9606.fasta; downloaded on 09/10/2018) with common serum contaminants and enzyme sequences. False discovery rate (FDR) was set to 1% at both the peptide spectrum match (PSM) and protein level. A minimum peptide count required for protein quantification was set to two. Protein groups were further analyzed using the Perseus software suite (Tyanova *et al.*, Nature Methods, 2016). Common contaminants, reverse proteins and proteins only identified by site were filtered out. LFQ values were transformed to $\log_2$ space and intensity distributions were checked to ensure that data was normally distributed.

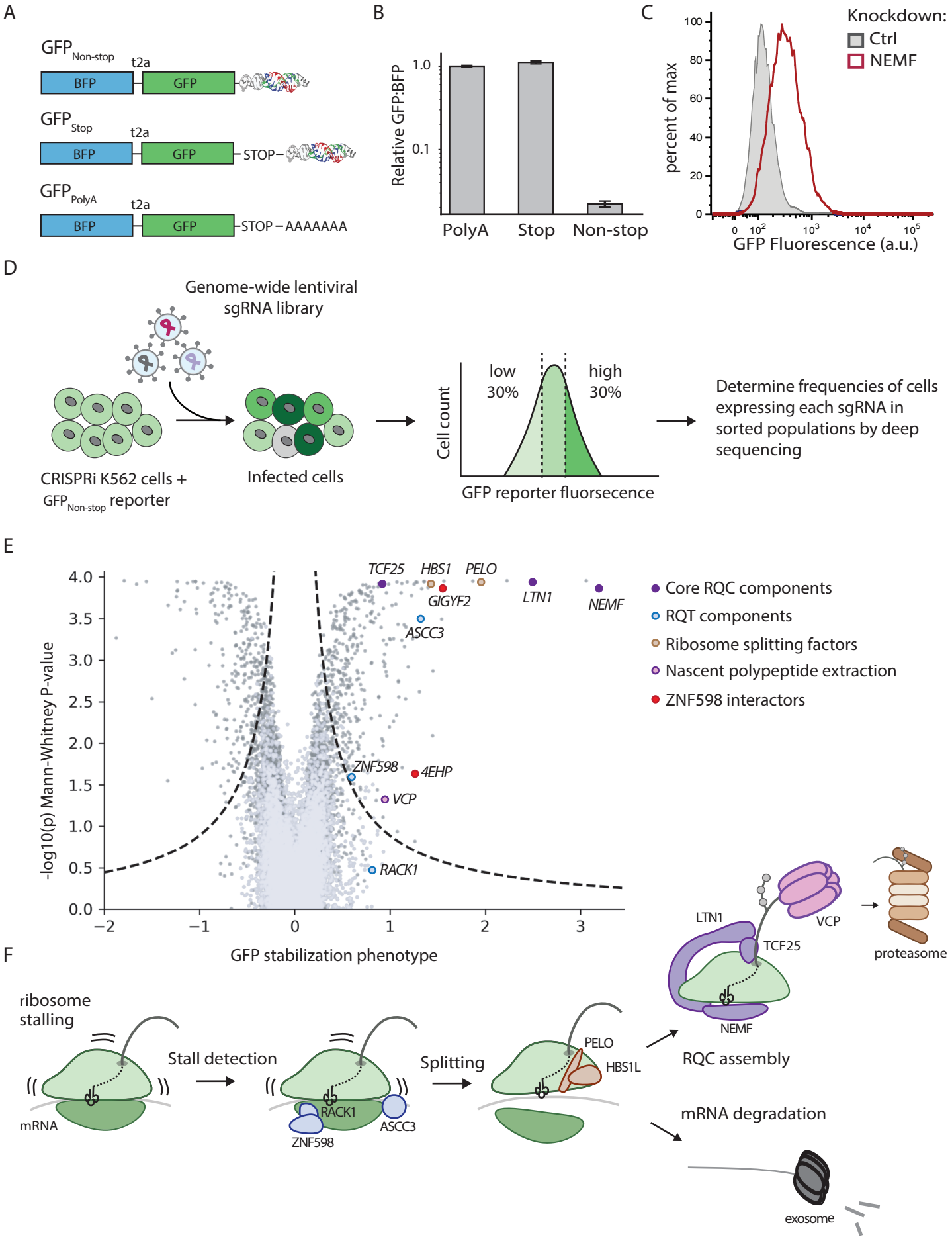
A
GFP Non-stop
t2a
BFP
GFP
GFP Stop
STOP
GFP PolyA
STOP – AAAAAAA
B
Relative GFP:BFP
1.0
0.1
PolyA
Stop
Non-stop
C
Knockdown:
Ctrl
NEMF
percent of max
GFP Fluorescence (a.u.)
D
Genome-wide lentiviral sgRNA library
CRISPRi K562 cells + GFP Non-stop reporter
Infected cells
Cell count
low 30%
high 30%
GFP reporter fluorescence
Determine frequencies of cells expressing each sgRNA in sorted populations by deep sequencing
E
-log10(p) Mann-Whitney P-value
GFP stabilization phenotype
TCF25
HBS1
PELO
GIGYF2
LTN1
NEMF
ASCC3
ZNF598
4EHP
VCP
RACK1
Core RQC components
RQT components
Ribosome splitting factors
Nascent polypeptide extraction
ZNF598 interactors
F
ribosome stalling
mRNA
Stall detection
RACK1
ASCC3
ZNF598
Splitting
PELO
HBS1L
LTN1
VCP
TCF25
NEMF
proteasome
RQC assembly
mRNA degradation
exosome

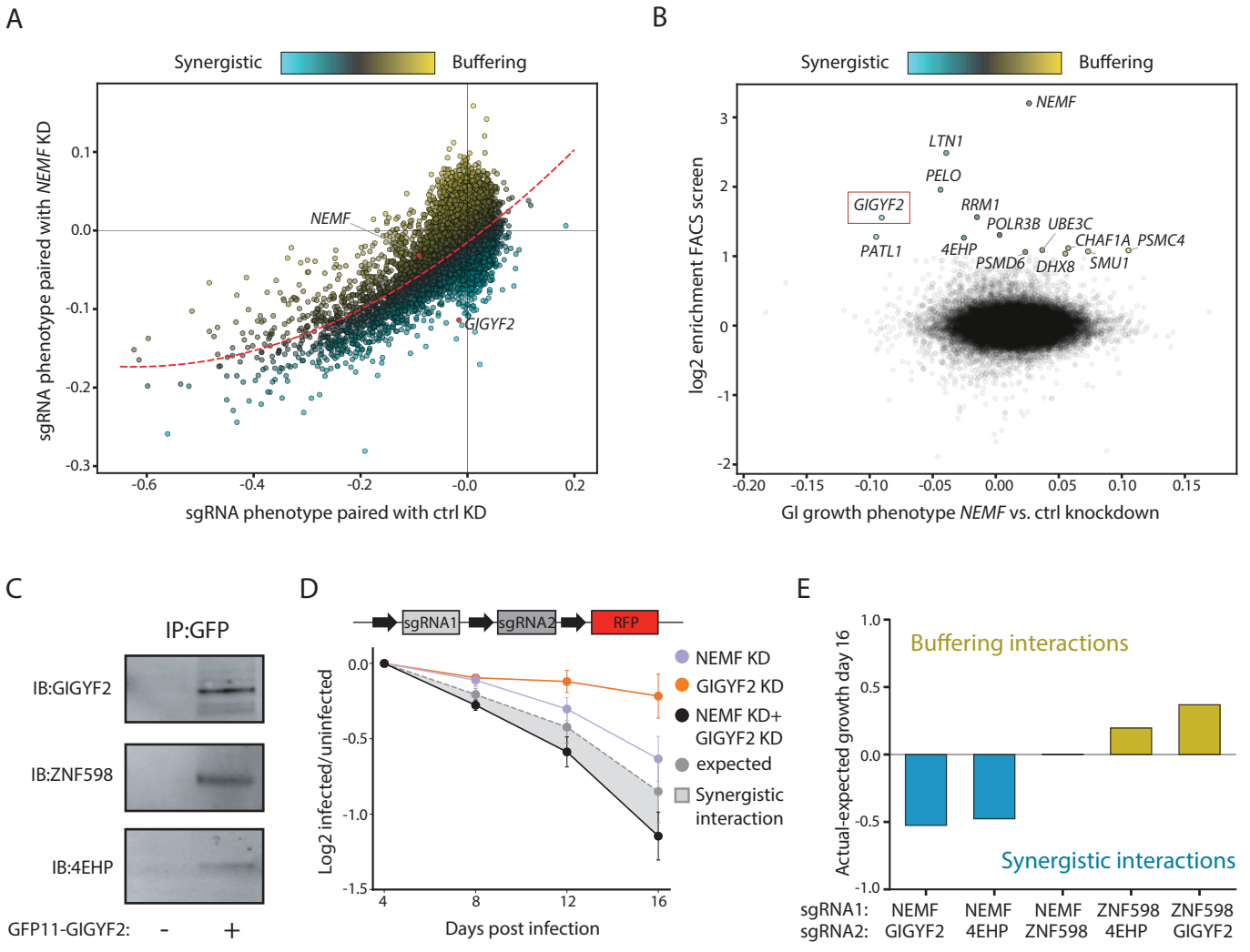
A
Synergistic
Buffering
sgRNA phenotype paired with NEMF KD
sgRNA phenotype paired with ctrl KD
NEMF
GIGYF2
B
Synergistic
Buffering
log2 enrichment FACS screen
GI growth phenotype NEMF vs. ctrl knockdown
NEMF
LTN1
PELO
GIGYF2
RRM1
POLR3B
UBE3C
CHAF1A
PSMC4
PATL1
4EHP
PSMD6
DHX8
SMU1
C
IP:GFP
IB:GIGYF2
IB:ZNF598
IB:4EHP
GFP11-GIGYF2: - +
D
sgRNA1
sgRNA2
RFP
Log2 infected/uninfected
Days post infection
NEMF KD
GIGYF2 KD
NEMF KD+ GIGYF2 KD
expected
Synergistic interaction
E
Buffering interactions
Synergistic interactions
Actual-expected growth day 16
sgRNA1: NEMF NEMF NEMF ZNF598 ZNF598
sgRNA2: GIGYF2 4EHP ZNF598 4EHP GIGYF2

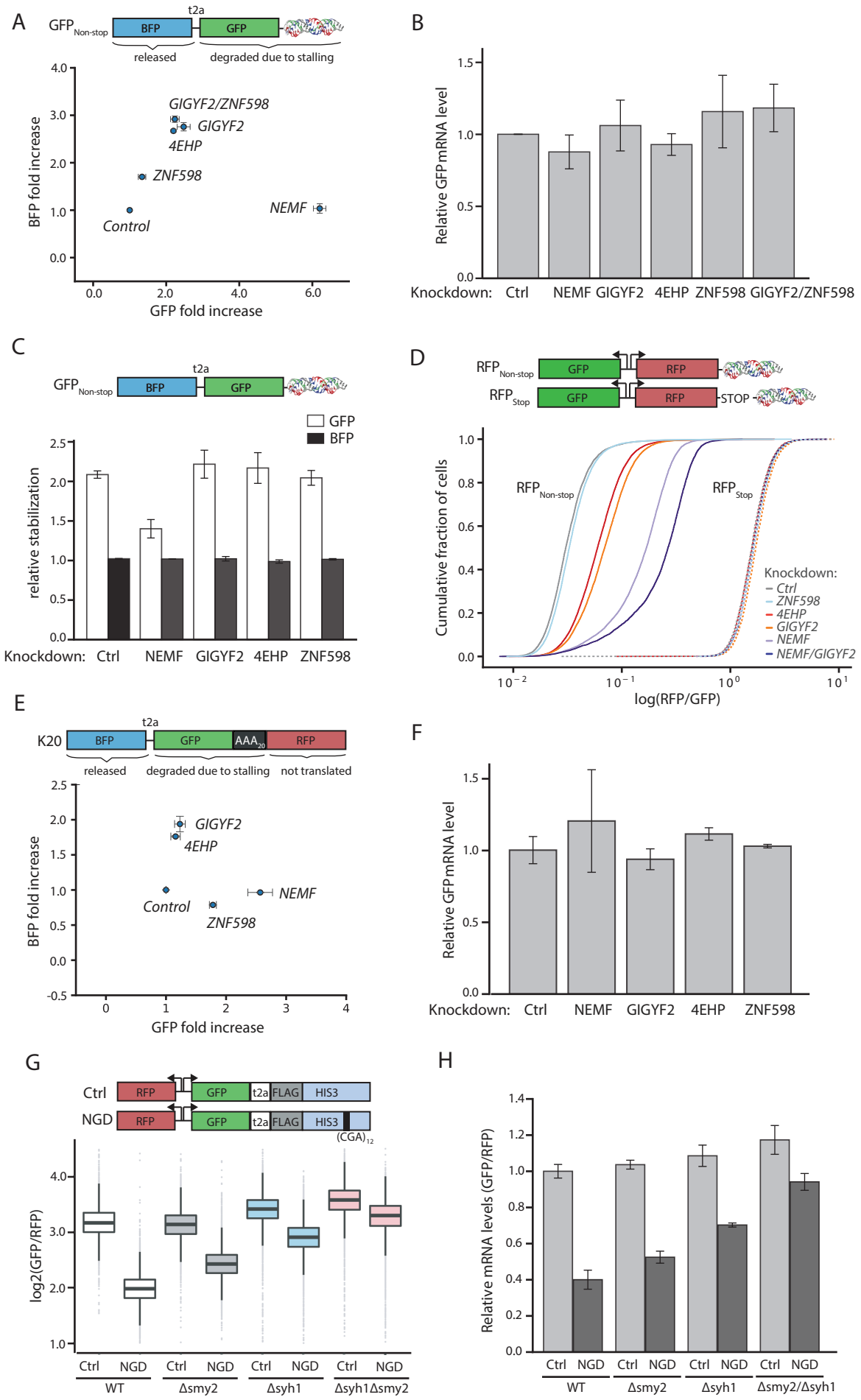
A
GFP Non-stop
t2a
BFP
GFP
released
degraded due to stalling
BFP fold increase
GFP fold increase
GIGYF2/ZNF598
GIGYF2
4EHP
ZNF598
NEMF
Control
B
Relative GFP mRNA level
Knockdown: Ctrl NEMF GIGYF2 4EHP ZNF598 GIGYF2/ZNF598
C
GFP Non-stop
t2a
BFP
GFP
relative stabilization
Knockdown: Ctrl NEMF GIGYF2 4EHP ZNF598
D
RFP Non-stop
RFP Stop
GFP
RFP
STOP
Cumulative fraction of cells
log(RFP/GFP)
Knockdown:
Ctrl
ZNF598
4EHP
GIGYF2
NEMF
NEMF/GIGYF2
E
K20
t2a
BFP
GFP
AAA20
RFP
released
degraded due to stalling
not translated
BFP fold increase
GFP fold increase
GIGYF2
4EHP
NEMF
Control
ZNF598
F
Relative GFP mRNA level
Knockdown: Ctrl NEMF GIGYF2 4EHP ZNF598
G
Ctrl
NGD
RFP
GFP
t2a
FLAG
HIS3
(CGA)12
log2(GFP/RFP)
Ctrl NGD Ctrl NGD Ctrl NGD Ctrl NGD
WT Δsmy2 Δsyh1 Δsyh1Δsmy2
H
Relative mRNA levels (GFP/RFP)
Ctrl NGD Ctrl NGD Ctrl NGD Ctrl NGD
WT Δsmy2 Δsyh1 Δsmy2/Δsyh1

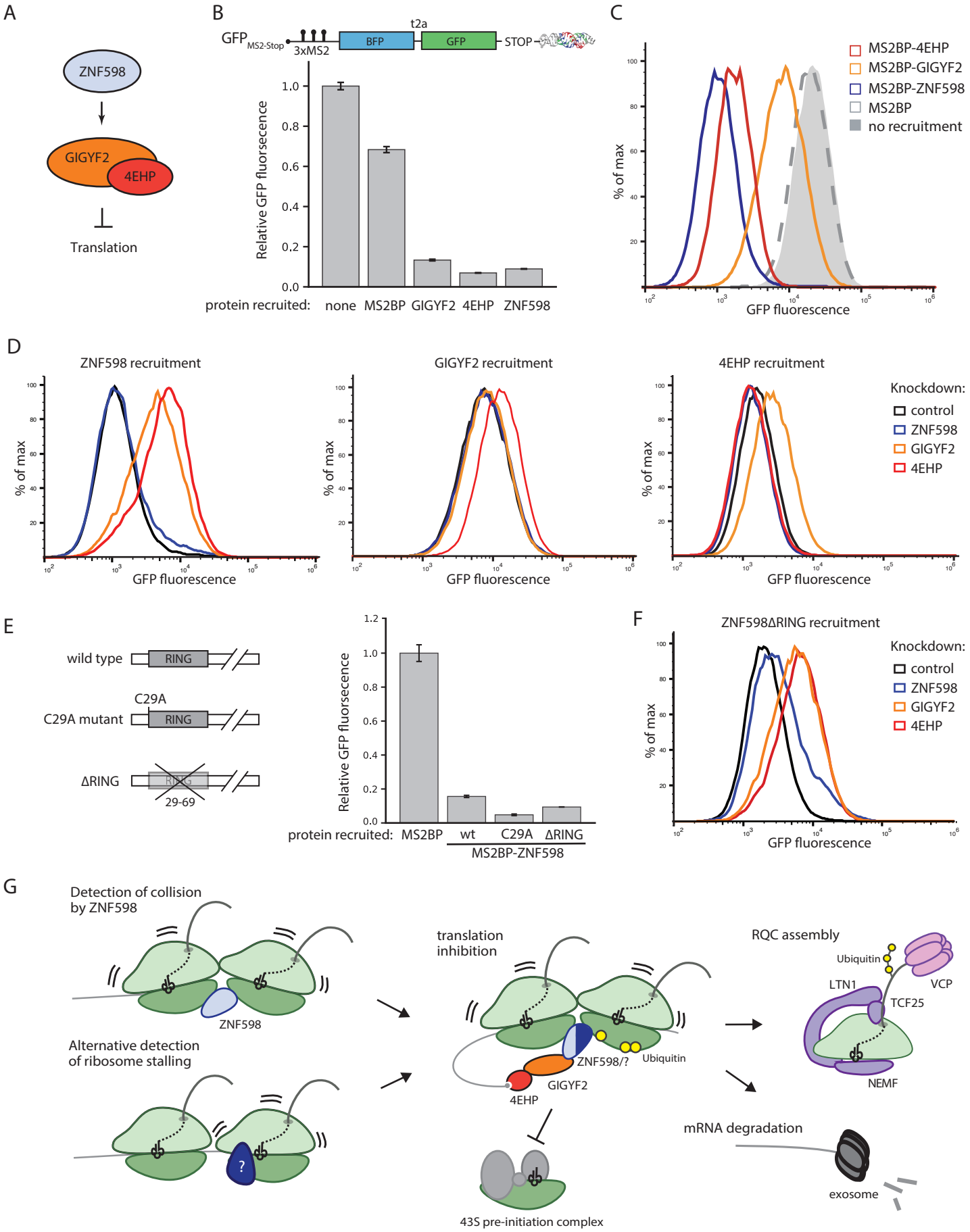
A
ZNF598
GIGYF2
4EHP
Translation
B
GFP
MS2-Stop
3xMS2
BFP
t2a
GFP
STOP
Relative GFP fluorescence
protein recruited:
none
MS2BP
GIGYF2
4EHP
ZNF598
C
MS2BP-4EHP
MS2BP-GIGYF2
MS2BP-ZNF598
MS2BP
no recruitment
% of max
GFP fluorescence
D
ZNF598 recruitment
GIGYF2 recruitment
4EHP recruitment
Knockdown:
control
ZNF598
GIGYF2
4EHP
% of max
GFP fluorescence
E
wild type
RING
C29A
C29A mutant
ΔRING
29-69
Relative GFP fluorescence
protein recruited:
MS2BP
wt
C29A
ΔRING
MS2BP-ZNF598
F
ZNF598ΔRING recruitment
Knockdown:
control
ZNF598
GIGYF2
4EHP
% of max
GFP fluorescence
G
Detection of collision
by ZNF598
ZNF598
Alternative detection
of ribosome stalling
translation
inhibition
ZNF598/?
Ubiquitin
GIGYF2
4EHP
43S pre-initiation complex
RQC assembly
Ubiquitin
VCP
LTN1
TCF25
NEMF
mRNA degradation
exosome